Electronic Supporting Information

Radiations of the high-order plasmonic modes of large gold nanospheres excited by surface plasmon polaritons

Jing-Dong Chen,[‡a] Jin Xiang,[‡a] Shuai Jiang,[a] Qiao-Feng Dai,[a] Shao-Long Tie,[b] and Sheng Lan[*a]

[a] Guangdong Provincial Key Laboratory of Nanophotonic Functional Materials and Devices, School of Information and Optoelectronic Science and Engineering, South China Normal University, Guangzhou 510006, China

[b] School of Chemistry and Environment, South China Normal University, Guangzhou 510006, China

[‡] These authors contributed equally to this work.

[*] E-mail: slan@scnu.edu.cn

Table of contents

1. Scattering spectra and radiation patterns of large gold nanospheres

Based on Mie theory, the electric quadrupole (EQ) and even octapole (EOC) of a large gold nanosphere (GNS) may appear in the visible light spectrum. In this case, the coherent interaction between the ED and EQ resonances (e.g., in a GNS with $d = 340$ nm) or that between the EQ and EOC resonances (e.g., in a GNS with $d = 560$ nm) will lead to highly directional radiation. In Fig. S1, we show the spectra of total scattering, forward scattering and backward scattering calculated for a GNS in air with a diameter of $d = 560$ nm. The resonance wavelengths of ED, EQ, and EOC determined by Mie theory are marked in the spectrum of total scattering. It is noticed that the forward scattering is much stronger than the backward one at the EQ and EOC resonances, implying the existence of highly directional radiation. In Fig. S1b,c,d, we show the three-dimensional (3D) radiation patterns calculated at the EOC, EQ, and ED resonances, respectively. Highly directional radiation in the forward direction is observed at the EQ resonance and it becomes more significant at the EOC resonance. This feature is clearly illustrated in Fig. S1e where a comparison of the two-dimensional (2D) radiation pattern on the *xz* plane at the ED, EQ, and EOC resonances is presented.
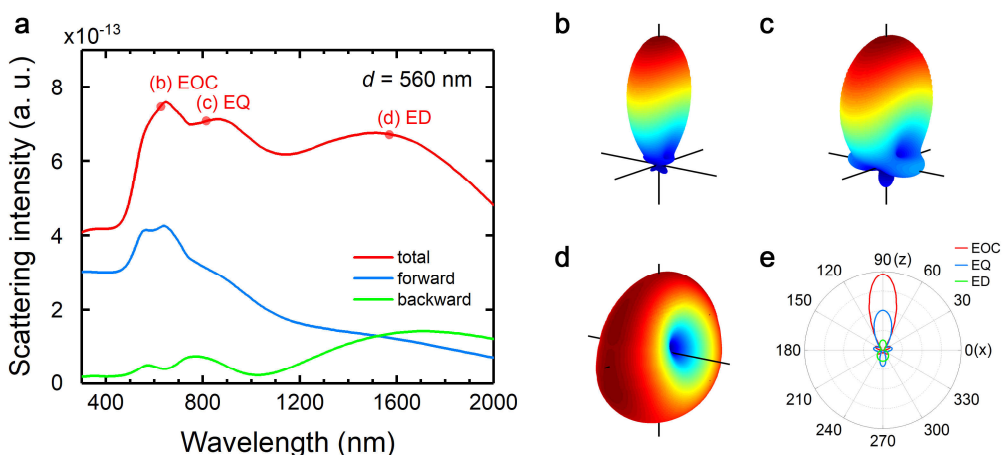

Fig. S1 (a) Scattering spectra, including total, forward and backward scattering, calculated for a GNS with $d = 560$ nm. The 3D radiation patterns calculated at the EOC, EQ, and ED resonances (620 nm, 810 nm, and 1570 nm) are presented in (b), (c), and (d), respectively. The 2D radiation patterns on *xz* plane at the EOC, EQ, and ED resonances are compared in (e).

2. Broadband surface plasmon polaritons generated by using slightly focused white light

In both experiments and numerical simulations, we used slightly focused white light to generate broadband SPPs which can be used to excite GNSs more efficiently as compared with the collimated white light. In Fig. S2, we show the reflection spectra measured for the SPPs by using collimated and slightly focused white light at an incidence angle of 45.8°. It can be seen that the bandwidth of the SPPs excited by using slightly focused white light is slightly broadened. Moreover, the reduction of the excitation spot diameter from

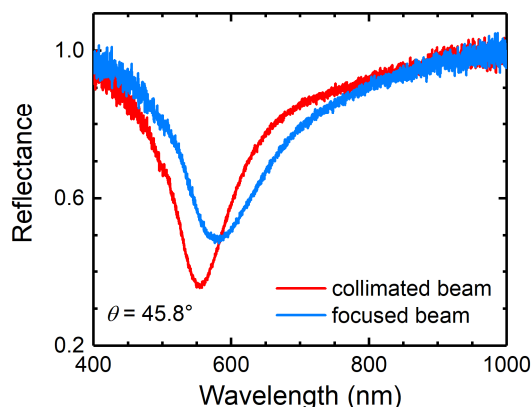~6 mm to ~2 mm significantly enhance the scattering light intensities of GNSs.

Fig. S2 Comparison of the reflection spectra measured for the SPPs by using collimated and slightly focused white light at an incidence angle of 45.8°.

3. Scanning electron microscopy images of gold nanospheres fabricated on a thin gold film

The GNSs used in our experiments were fabricated by using femtosecond (fs) laser ablation of a 50-nm-thick gold (Au) film deposited on a silica substrate. High-quality GNSs with spherical shapes and smooth surfaces randomly distributed on the thin Au film were successfully obtained, as shown in Fig. S3 where the scanning electron microscopy (SEM) images of the GNSs are presented. In Fig. S4, we show the scattering light of randomly distributed GNSs observed by using conventional dark-field microscopy and recorded by using a charge coupled device (CCD).
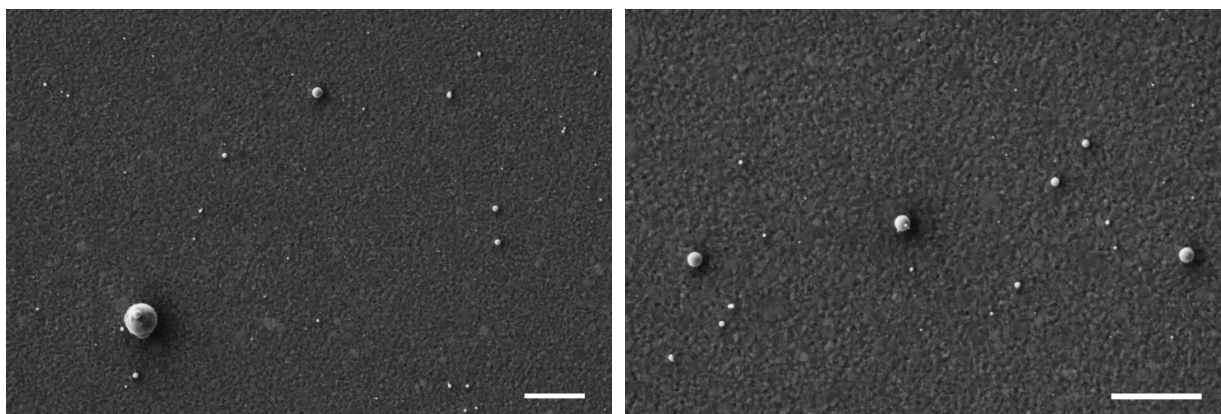

Fig. S3 SEM images of GNSs with different diameters fabricated on a 50-nm-thick Au film by using fs laser ablation. In both cases, the length of the scale bar is 1.0 μm.
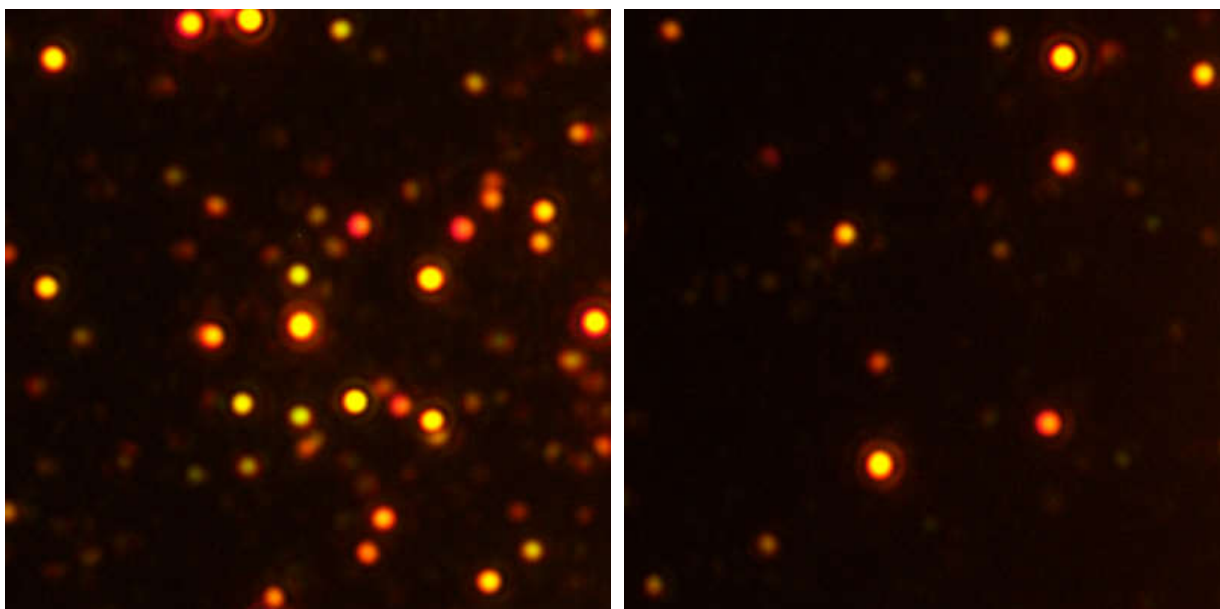
Fig. S4 CCD images of the randomly distributed GNSs observed by using conventional dark-field microscopy.

4. Evolution of the scattering spectrum of a gold nanosphere with increasing diameter

In order to see the emergence of the EQ and EOC resonances in the visible light spectrum and the evolution of the ED, EQ, and EOC resonances with increasing diameter of a GNS, we have calculated the evolution of the scattering spectrum of a GNS placed on a silica substrate, including total and forward scattering, with increasing diameter by using the finite-difference time domain (FDTD) method, as shown in Fig. S5. It can be seen that a large red shift of the ED resonance occurs for GNSs with $d > 250$ nm. Meanwhile, the EQ resonance emerges in the visible light spectrum for GNSs with $d > 220$ nm. In addition, the EOC resonance appears in the visible light spectrum for GNSs with $d > 380$ nm.
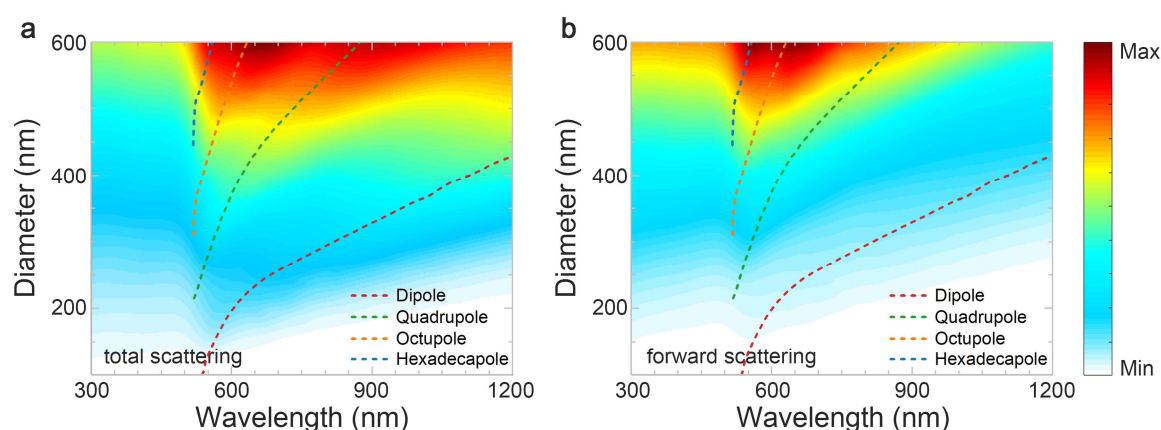

Fig. S5 Evolution of the ED, EQ, and EOC resonances of a GNS with increasing diameter in the total scattering spectrum (a) and forward scattering spectrum (b).

5. Mirror-image-induced magnetic dipole

Owing to the existence of the thin Au film, the coherent interaction between p_x and its mirror image p_{xm} will generate a magnetic dipole (m_y) at the contacting point between the GNS and the Au film. In Fig. S6a, we show the scattering spectrum measured and calculated for a GNS with $d = 240$ nm where two scattering peaks are observed. While the scattering peak at the short wavelength of ~530 nm originates from the peak transmission of the Au film, the scattering peak at the long wavelength of ~800 nm is attributed to the radiation of m_y. In order to verify this assignment, we calculated the magnetic field distribution on the xz plane at 800 nm, as shown in Fig. S6b. It can be seen that the strongest magnetic field is achieved at the contacting point between the GNS and the Au film.
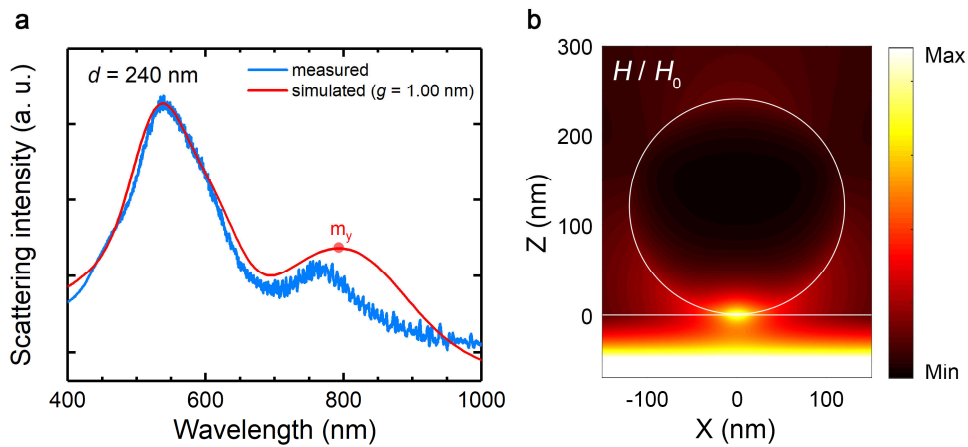

Fig. S6 (a) Scattering spectrum measured and calculated for a GNS with $d = 240$ nm placed on a 50-nm-thick Au film. (b) Magnetic field distribution on the xz plane calculated at 800 nm. The gap width between the GNS and the Au film was assumed to be $g = 1.00$ nm.

6. Gap plasmon modes induced in large gold nanospheres

As mentioned above, the scattering intensity of m_y is usually much stronger than those of other dipole plasmon modes, such as the gap plasmon mode g_x, due to the significantly enhanced magnetic field at the contacting point between the GNS and the Au film. As a result, the radiation of g_x is usually invisible in the scattering spectrum. However, it may appear as a small shoulder in some cases. In Fig. S7a, we show the scattering spectrum measured and simulated for a GNS with $d = 240$ nm. A small shoulder is observed at ~680 nm and it is caused by the radiation of g_x. This assignment is verified by the electric field distribution on the xz plane calculated at 680 nm, as shown in Fig. S7b.
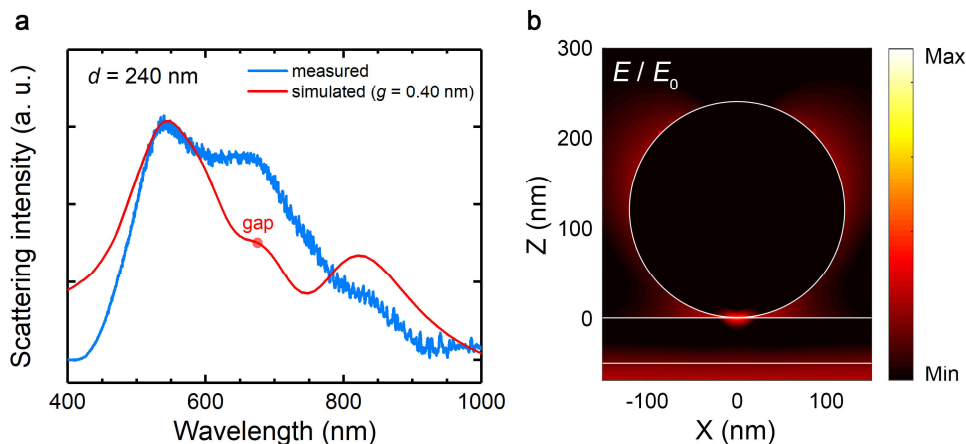
Fig. S7 (a) Scattering spectrum measured and calculated for a GNS with d = 240 nm placed on a 50-nm-thick Au film. (b) Electric field distribution on the xz plane calculated at 680 nm. The gap width between the GNS and the Au film was assumed to be g = 0.40 nm.

7. Influence of the Au film on the scattering spectra of large gold nanospheres

The scattering spectra presented in this work were normalized by using the spectrum of the illumination light as reference. However, a transmission peak was observed in the transmission spectrum of the Au film, as shown in Fig. S8. The existence of such a transmission peak influences the scattering spectra of GNSs measured by using conventional dark-field microscopy because GNSs were excited by the evanescent wave on the front surface of the Au film. As a result, a scattering peak ~530 nm was observed in the scattering spectra of all GNSs (see Fig. 2 and Fig. S8) and it remained nearly unchanged when the diameter of the GNS was increased. If the scattering spectra of the GNSs are normalized by using the transmission spectrum of the Au film instead of the spectrum of the illumination light, then the scattering peak at ~530 nm becomes a small shoulder or disappears completely, as shown in Fig. S8.
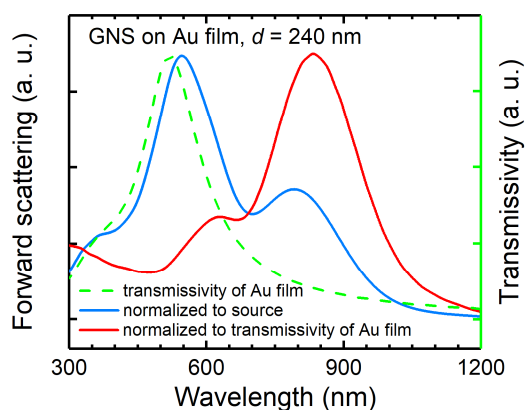

Fig. S8 Scattering spectrum calculated for a GNS with d = 240 nm placed on a 50-nm-thick Au film. The transmission spectrum of the 50-nm-thick Au film is also provided for reference. The gap width between the GNS and the Au film was

assumed to be $g = 1.00$ nm.

The above argument can be further verified by examining the scattering spectrum of a GNS placed on a thin Ag film. In this case, the scattering peak at the short wavelength appears at ~330 nm and it disappears when the scattering spectrum is normalized by using the transmission spectrum of the Ag film, as shown in Fig. S9.
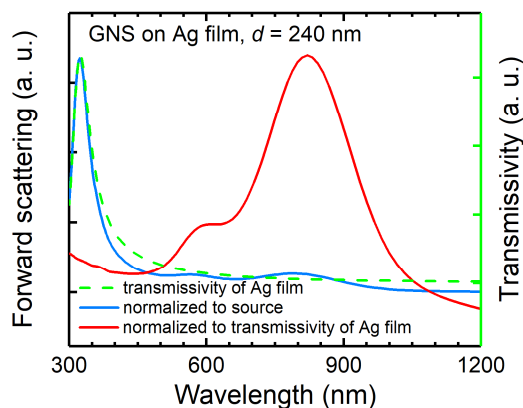

Fig. S9 Scattering spectrum calculated for a GNS with $d = 240$ nm placed on a 50-nm-thick Ag film. The transmission spectrum of the 50-nm-thick Ag film is also provided for reference. The gap width between the GNS and the Ag film was assumed to be $g = 1.00$ nm.

8. Enhancement of electric field on the surface of the gold film by surface plasmon polaritons

As discussed in the main text, high-order plasmon modes are difficult to be resolved in conventional dark-field microscopy because the GNSs are excited by the evanescent wave which has been attenuated significantly after passing through the Au film. In sharp contrast, a significantly enhanced electric field is created on the surface of the Au film, which is quite suitable for exciting the EQ and EOC of a large GNS, when the surface plasmon polaritons (SPPs) on the surface of the Au film are excited, as shown in Fig. S10.
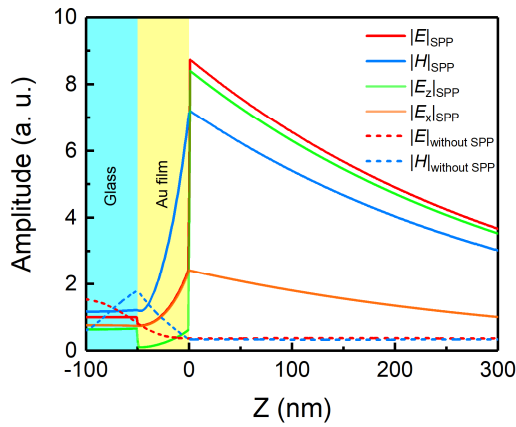
Fig. S10 Comparison of the electric field enhancement on the surface of a 50-nm-thick Au film with ($\theta = 45.8°$) and without ($\theta = 0°$) the excitation of the SPPs.

9. Fitting of the scattering spectra of gold nanospheres

In Fig. S11, we show the scattering spectra measured for GNSs with different diameters excited by using the SPPs generated on the surface of the Au film. During the measurements, the polarization angle of the polarization analyzer was varied from 0° to 90° with an increment of 10°. Each spectrum was fitted by using multiple Lorentz line shapes corresponding to different plasmon modes. Very good agreement between the measured spectra and the fitting results was observed.
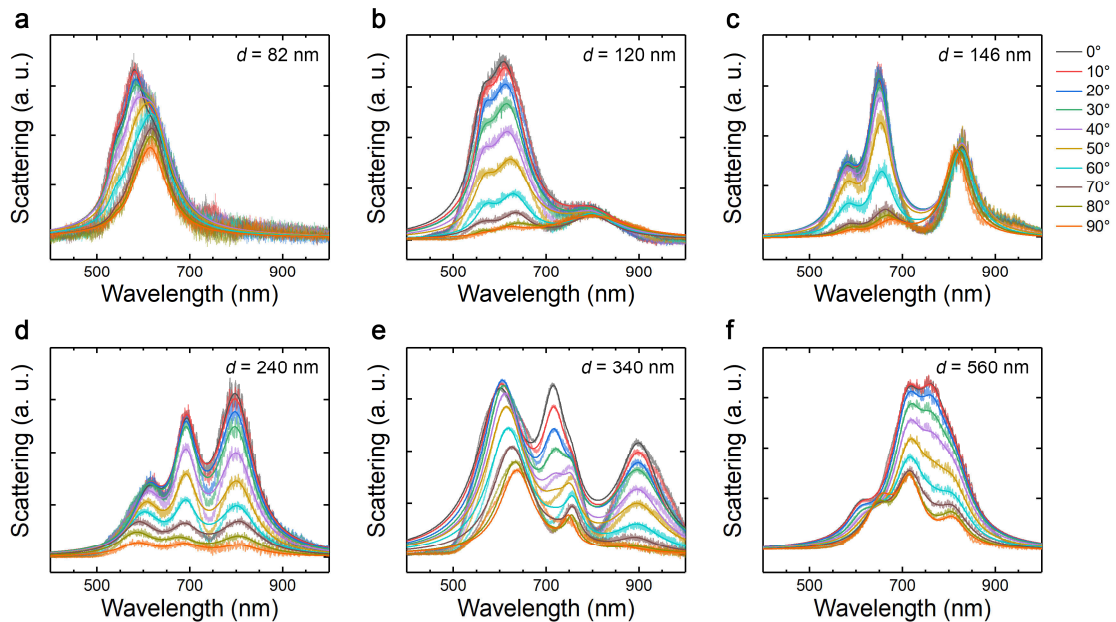

Fig. S11 Scattering spectra measured for SPPs-excited GNSs with different diameters of (a) $d = 82$, (b) $d = 120$, (c) $d = 146$, (d) $d = 240$, (e) $d = 340$, and (f) $d = 560$ nm by setting the polarization analyzer at different polarization angles from 0° to 90° with an interval of 10°. The fittings of the polarization-dependent scattering spectra by using multiple Lorentz line shapes corresponding to different modes are also provided.

In order to identify the plasmon modes which are responsible for the scattering peaks observed in the scattering spectra of GNSs with different diameters, we have fitted the scattering spectra measured at different polarization angles by using multiple Lorentz line shapes, as shown in Fig. S12. In this way, the angular-dependences of the scattering intensity can be extracted for different plasmon modes excited in large GNSs.
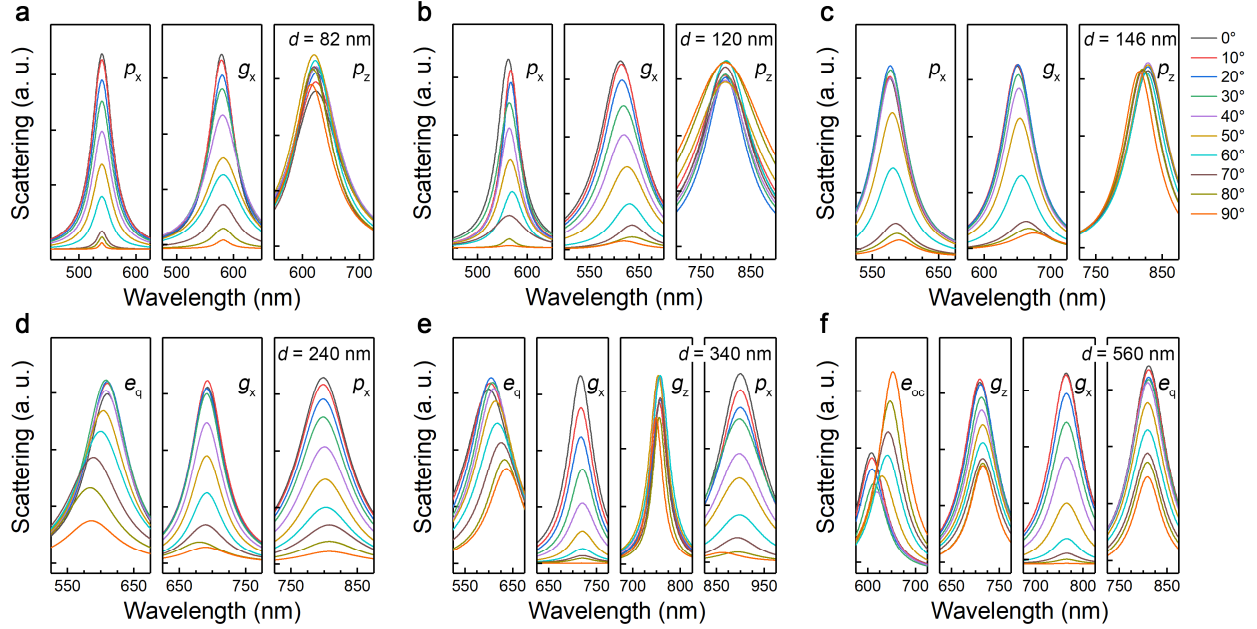

Fig. S12 Fitting of the scattering spectra with multiple Lorentz line shapes corresponding to different plasmonic modes for SPPs-excited GNSs with different diameters of (a) $d = 82$, (b) $d = 120$, (c) $d = 146$, (d) $d = 240$, (e) $d = 340$, and (f) $d = 560$ nm.

10. Decomposition of the scattering spectra of large gold nanospheres based on Mie theory

The total scattering spectra of a large GNS can be decomposed into the contribution of ED, EQ, EOC and EHEX based on the Mie theory. In Fig. 13, we show the decompositions of the scattering spectra calculated for two large GNSs with $d = 340$ nm and $d = 560$ nm. For the GNS with $d = 340$ nm shown in Fig. S13a, a large overlap between the ED and EQ resonances is observed. In addition, there exists a small overlap between the EQ and EOC resonances. In the fitting of the polarization-dependent scattering spectra measured for the GNS with $d = 340$ nm, we did not consider the contribution of the EOC. As a result, a red shift of the resonant wavelength of e_q with increasing the polarization angle was observed (see Fig. S12e). Similarly, a large overlap of the EQ and EOC resonances is found for the GNS with $d = 560$ nm, as shown in Fig. S13b. In addition, a relatively small overlap is observed for the EQ and EHEX resonances and also for the EOC and EHEX resonances. Since the contribution of the EHEX to the scattering was not taken into account in the fitting of the polarization-dependent scattering spectra of the GNS, a red shift of the resonant wavelength of e_{oc} was observed when the polarization angle was increased (see Fig. S12f).
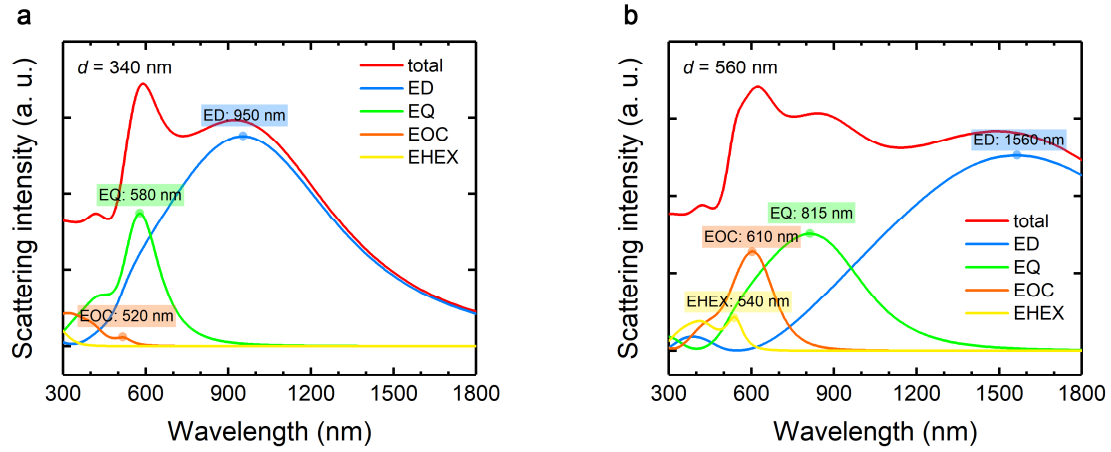
Fig. S13 Decomposition of the total scattering spectra into the contributions of ED, EQ, EOC and EHEX calculated for GNSs with d = 340 nm (a) and d = 560 nm (b) based on Mie theory.

11. Enhancement of electric field calculated for gap plasmon modes excited by surface plasmon polaritons

The enhancement of electric field at the contacting point for the gap plasmon mode (g_z) depends strongly on the gap width g between the GNS and the Au film. In Fig. S14, we show the wavelength dependence of the electric field enhancement factor calculated for two GNSs of d = 150 and 240 nm with different gap widths. In both cases, it can be seen that the enhancement factor increases rapidly with decreasing gap width.
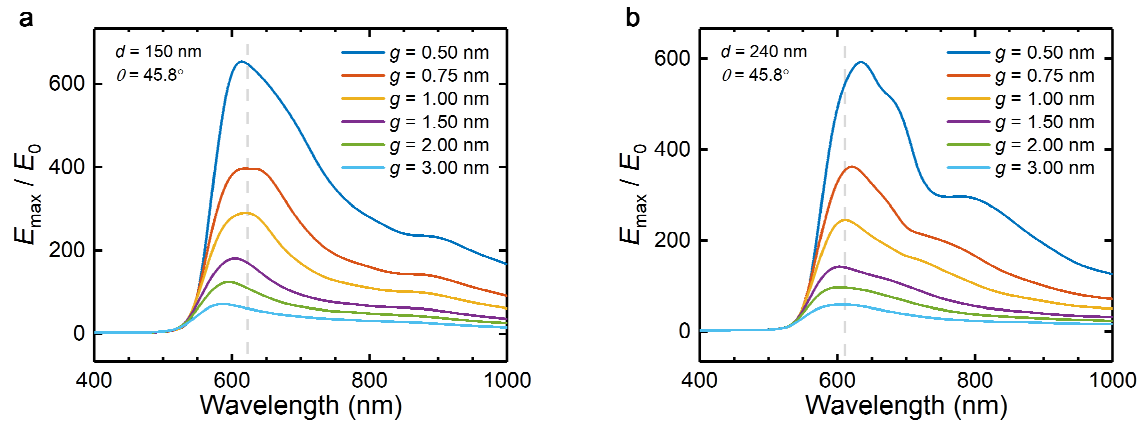

Fig. S14 Wavelength dependence of the electric field enhancement factor at the contact point between the GNS and the Au film calculated for two GNSs with (a) d = 150 nm and (b) d = 240 nm.